Catalysis Today 419 (2023) 114163

Contents lists available at ScienceDirect

Catalysis Today

journal homepage: www.elsevier.com/locate/cattod

Light-driven urea oxidation for a wearable artificial kidney

Jeroen C. Vollenbroek [a,b,*], Ainoa Paradelo Rodriguez [c], Bastian T. Mei [c,d], Guido Mul [c], Marianne C. Verhaar [a], Mathieu Odijk [b], Karin G.F. Gerritsen [a]

[a] Nephrology and hypertension department, UMC Utrecht, Heidelberglaan 100, 3584 CX Utrecht, the Netherlands
[b] BIOS Lab on a Chip Group, MESA+ Institute, University of Twente, Hallenweg 15, 7522 NH Enschede, the Netherlands
[c] Photocatalytic Synthesis (PCS) group, University of Twente, Drienerlolaan 5, 7522 NB Enschede, the Netherlands
[d] Industrial Chemistry, Ruhr-University Bochum, Universitätsstr. 150, 44801 Bochum, Germany

ARTICLE INFO

Keywords:
Wearable artificial kidney
Photo-electrocatalysis
Selective urea oxidation

ABSTRACT

For the development of a wearable artificial kidney (WAK) that uses a small dialysate volume that is continuously regenerated, it is essential that urea, one of the main uremic retention solutes, is removed. Despite advances in sorbent technology or electro-oxidation no safe, efficient and selective method for urea removal has been reported that allows miniaturization of the artificial kidney to wearable proportions. Here we have developed a flow cell for light-driven, photo-electrocatalytic (PEC) urea removal for use in a WAK. We use a photo-active material (hematite) coated with a catalyst (NiOOH) as working electrode for selective urea oxidation and a silver-chloride (AgCl) cathode. The use of the AgCl counter electrodes eliminates the need for an external bias voltage, and allows operation under light illumination only. Using LED illumination (460 nm) we show that urea is selectively oxidized over chloride. N_2 formation is confirmed by gas-phase analysis of the headspace of the sample vial, using mass spectrometry. Other nitrogen containing products include nitrite but importantly ammonia and nitrate are not detected. Using the PEC concept a urea removal rate of 2.5 μmol/cm^{2}h (or 0.15 mg/cm^{2}h) has been achieved. Extrapolating our results to an upscaled system, a surface area of 0.5 m^2 would enable efficient removal of the daily produced amount of urea (~300 mmol) urea within 24 h, when driven by LED illumination only.

1. Introduction

Patients suffering from chronic kidney decease (CKD) undergo life-saving dialysis treatment in the hospital or dialysis clinic 3 times a week for 4 h. This heavily reduces the patients' autonomy and quality of life. A Wearable Artificial Kidney (WAK) would considerably contribute to the patients' wellbeing, as prolonged and continuous treatment, without the need to go the hospital or dialysis clinic will increase both the efficiency and the comfort of the treatment [1,2]. A WAK requires a small volume of dialysis fluid and subsequent regeneration. During regeneration the extracted toxins are removed from the spent dialysate. One of the most difficult to remove molecules form the spent dialysate is urea. Urea is the main waste product from protein metabolism and CKD patients have elevated plasma urea concentrations between 20 and 30 mM [1]. The REcirculation DialYsis (REDY) sorbent system is most commonly in use for sorbent based dialysis. In this system urea the enzyme urease is used to convert urea into ammonium (among others) and sorbents are required to capture the formed ammonium. However, the REDY system cannot bind urea directly and ammonium is more toxic than urea [1,3]. Other sorbent systems aiming at direct urea binding are mostly hampered by sluggish binding kinetics of urea and the competition of water for the active binding sites [1,4,5]. Therefore, electro-oxidation (EO) could be an attractive method to remove toxic retention solutes from the spent dialysate. EO devices are considered small, lightweight, durable, reusable and can be made from relatively cheap and earth abundant materials [1,6,7]. However, current EO systems are not selective for urea removal and toxic by-products such as chlorine, chloramines and hypochlorous acid are formed [1,8,9]. Considering that chloride is the most prevalent anion in the human body as well as in spent dialysate it is important to suppress chloride oxidation. Furthermore, glucose oxidation products that are additionally formed cause bio-incompatibility [8]. Recently, the use of titanium dioxide (TiO_2) photo-electrodes has been reported for the purpose of spent dialysate regeneration[10]. However, TiO_2 itself has been shown to have

* Corresponding author at: Nephrology and hypertension department, UMC Utrecht, Heidelberglaan 100, 3584 CX Utrecht, the Netherlands.
E-mail address: j.c.vollenbroek@umcutrecht.nl (J.C. Vollenbroek).

https://doi.org/10.1016/j.cattod.2023.114163
Received 15 November 2022; Received in revised form 15 March 2023; Accepted 24 April 2023
Available online 25 April 2023

poorer selectivity for urea oxidation over chloride oxidation and some chlorine by-products are still measured and produced [10] .Furthermore, bare TiO_2 shows no distinct oxidation peak for urea [9,11,12]. Due to the poor selectivity that is generally observed in electrochemical oxidation of urea, the use of (photo)-electrocatalytic (PEC) systems has been suggested as an alternative approach [13–16], using a process scheme as depicted in Fig. 1.

Research focused on green and efficient hydrogen production, as well as waste water treatment [13,15,17] has shown that it is more energy efficient to have urea oxidation as a counter reaction than the typically used oxygen evolution reaction. The oxygen evolution reaction has a thermodynamic potential of ~1.23 V versus ~0.37 V for the urea oxidation [13,18]. Using a nickel (Ni) based catalysts in combination with photosensitive materials such as hematite (Fe_2O_3) or TiO_2, it is shown that the combination of a photo-sensitive material and catalyst can enhance the selectivity for urea oxidation [13–15]. Hematite is of interest due to its abundance and inherent stability in pH neutral and alkaline environments [14,15]. Furthermore, the bandgap of hematite allows for visible (blue) light utilization whereas TiO_2-based photoelectrodes rely on UV light excitation [14,15]. Bismuth vanadate ($BiVO_4$) is another frequently used photoanode. Yet despite its benefits in charge carrier transport leading to higher photo-currents, $BiVO_4$ is not stable and dissolves at the highly alkaline conditions required in the Ni-based (photo)-electrocatalytic processes for selective urea oxidation over chloride oxidation in a WAK [19,20].

Without the presence of the Ni catalyst and in pH neutral conditions, the required potential for urea oxidation falls in the range where both water splitting and chloride oxidation occur [1]. However, it has been shown that adding a catalyst can increase the selectivity for both water splitting and urea oxidation in saline solutions under highly alkaline conditions [21,22]. For water oxidation the increase is primarily caused by the pH-dependence of the thermodynamic potential contrasting the thermodynamic potential of 2-electron chloride oxidation [21]. In the case of urea oxidation the regeneration of the catalyst in alkaline conditions is important [23,24]. Hypochlorite formation from Cl^- and OH^- may cause a problem as it follows the same pH dependent behavior as the oxygen evolution reaction. However, the oxygen evolution reaction is still thermodynamically favored [22]. Given the fact that the urea oxidation reaction is more favorable than the oxygen evolution reaction [18,25], the formation of hypochlorite under these conditions is considered unlikely. Furthermore, it is found that Ni-based catalysts do not favor formation of ammonium and nitrate during urea oxidation [12]. The specific catalyst used is NiOOH of which one pathway is that the active sites react chemically with urea to form CO_2, N_2 and H_2O, [23,24] as shown in Eq. (1). After this reaction the catalyst is in a deactivated $Ni(OH)_2$ state. The catalyst is electrochemically regenerated by reacting with an OH^- ion at a potential of 0.49 V vs SHE[26] in highly alkaline conditions, Eq. (2). Other possible electrochemical reaction pathways that form nitrite or nitrate are given in eq3 and eq4 at − 0.166 V and − 0.126 V vs SHE, respectively [27]. In a PEC device that uses photosensitive materials such as hematite catalyst regeneration is aided by photo-generated holes (h^+), see Eq. (5), where the * indicates the photo-excited hematite. For fast and efficient catalyst reactivation a pH > 12 is required. The hydrogen evolution reaction occurs at a potential of − 0.83 V vs SHE [13,26], (Eq. 6). By changing the counter reaction of hydrogen evolution to a silver-chloride reduction (0.22 V vs SHE [28], Eq. 7), it is possible to perform the coupled redox reactions solely light-driven. When the AgCl layer is depleted the reaction should stop as silver cannot be further reduced. The induced photo-voltage provides enough energy for the redox reactions to occur. In the case of the hydrogen evolution reaction the overall potential that would be necessary for these reactions to occur (based on their standard potentials) is 1.32 V [26]. The overall potential between the AgCl cathode and the NiOOH/hematite anode would be reduced to 0.34 V. The process of the electron-hole pair generation and subsequent (electro)chemical reaction possibilities at the anode and cathode are given below. In previously

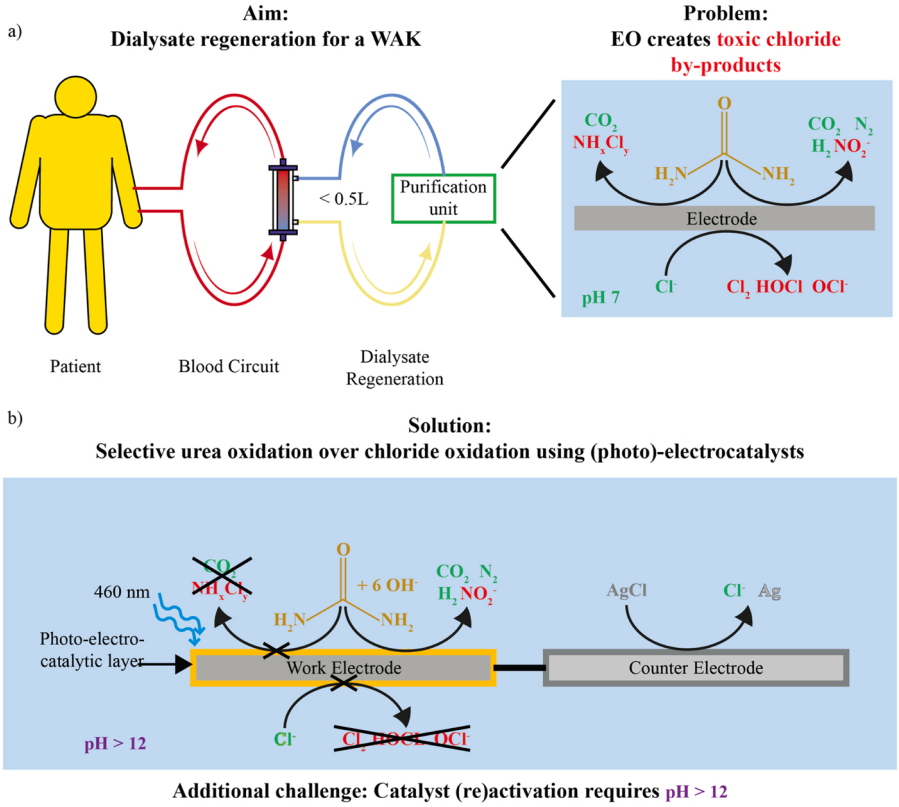

Fig. 1. a) The concept of a WAK using a small volume of dialysate that is continuously regenerated in a closed loop. b) the current problem of EO generated toxic by-products during urea oxidation (a) can be circumvented by using (photo)-electrocatalysts for increased selectivity.

used WAK systems both graphite and platinum counter electrodes were used that performed the oxygen evolution as counter reaction [1,6–8].

Chemical reaction between urea and the activated catalyst at the anode:

$$6\ NiOOH + urea + H_2O \rightarrow 6\ Ni(OH)_2 + CO_2 + N_2 \quad (1)$$

Electrochemical catalyst activation at the anode:

$$6\ Ni(OH)_2 + 6\ OH^- + 6\ h^+ \rightarrow 6\ NiOOH + 6\ H_2O\ E_0 = 0.49\ V\ vs\ SHE \quad (2)$$

Electrochemical pathways for nitrite and nitrate formation at the anode:

$$Urea + 16\ OH^- \rightarrow 2\ NO_2^- + CO_3^{2-} + 10\ H_2O + 12e^-\ E_0 = -0.166\ V\ vs\ SHE \quad (3)$$

$$Urea + 20\ OH^- \rightarrow 2\ NO_3^- + CO_3^{2-} + 12\ H_2O + 16e^-\ E_0 = -0.126\ V\ vs\ SHE \quad (4)$$

Photo-activation of hematite:

$$Fe_2O_3 + hv \rightarrow Fe_2O_3^* + h^+ + e^-\ \lambda = 460\ nm \quad (5)$$

Electrochemical hydrogen evolution at the cathode:

$$H_2O + 2\ e^- \rightarrow H_2 + 2\ OH^-\ E_0 = -0.83\ V\ vs\ SHE \quad (6)$$

Electrochemical silver chloride reduction at the cathode:

$$AgCl + e^- \rightarrow Ag + Cl^-\ E_0 = 0.22\ V\ vs\ SHE \quad (7)$$

For the use in a WAK, the necessity for reactivation of Ni-based catalysts in an alkaline medium still poses an additional challenge [13,23,24]. The highly alkaline environment is not compatible for use with patients. Creating a local alkaline environment without affecting the pH of the bulk solution (for example, by use of an additional fluidic loop separated from the bulk solution by a urea permeable OH^- impermeable cation exchange/anion rejection membrane) may solve this problem and is focus of future research. Since we consider the catalytic selectivity of the NiOOH/hematite system of urea oxidation over chloride oxidation of such a benefit, we here already report the use of a flow cell for light-driven urea decomposition, even though nitrite formation was observed with up to 39% Faradaic efficiency, indicating that further optimization of the system is required. Nevertheless, using a NiOOH/-hematite working electrode a urea removal rate of 2.5 μmol/cm^{2}h has been obtained. Importantly, we here also propose the use of AgCl cathodes to enable solely light-driven cell operation, i.e. without external bias. This can be of interest for generating energy from urea waste as well. For future development this could mean the device is (partially) solar operated, making more lightweight and energy friendly. The results presented here reveal the potential of photo-electrocatalytic systems for spent dialysate regeneration in a WAK.

2. Materials and methods

2.1. Electrode fabrication

2.1.1. Hematite synthesis

Glass slides with a conductive FTO coating (370 nm thick FTO, surface resistivity 7 Ω/cm^2, Sigma Aldrich) are used as the base material for the PEC electrodes. Deposition of the photosensitive hematite layer is done via a hydrothermal deposition method, as previously described by Xu et al. and further detailed in the supporting information [14]. In brief, the pH of 33 mL of a solution containing 0.15 M of $FeCl_3$6 H_2O (236489 ≥97%, Sigma Aldrich) and 1 M of $NaNO_3$ (S506 ≥99.0%, Sigma Aldrich) is adjusted with HCl (258148 37%, Sigma Aldrich) to a pH of 1.5. The solution and two substrates are loaded into a 50 mL Teflon vessel. of the autoclave (Techinstro). Using a Teflon holder, the substrates are angled towards the wall of the Teflon vessel with the conductive substrate facing downwards. Hydrothermal deposition takes place at 100 °C. The temperature is ramped up at a rate of 2 °C per minute and maintained for 12 h. Subsequently the substrate is cleaned using DI water and is annealed at 550 °C for 2 h also at a ramp of 2 °C per minute under atmospheric gas composition. An image of the used autoclave and images of the substrate after the deposition and annealing step are shown in the supporting information (see figure A.1 and A.2).

2.1.2. Nickel deposition

The hematite/FTO electrode is first cleaned in a 1 M NaOH (S8045 ≥98%, Sigma Aldrich) solution using cyclic voltammetry. Three scans are performed from 0 to 0.8 V vs a liquid junction Ag/AgCl (sat'd KCl) reference electrode (CH Instruments) and a Pt counter electrode at a scan rate of 50 mV/s, as previously described by Xu et al. [14] The cleaned substrate is put in a 0.1 M $NiNO_3$6 H_2O (72253 ≥97%, Sigma Aldrich) solution and a potentiometric deposition at − 0.65 V vs Ag/AgCl (sat'd KCl) is applied for 120 s using a Pt counter electrode.

2.1.3. AgCl counter electrode fabrication

For the counter electrode a piece of silver foil (0.1 mm 99.9%, Sigma Aldrich) is used as base material. Chlorination is done in a 3 M KCl solution (P5405 ≥ 99.0%, Sigma Aldrich) using a Pt counter electrode and a silver wire as quasi-reference electrode. For the chlorination of the silver foil an amperometric method with current density of 1 mA/cm^2 is used for 2 h.

2.2. PEC electrode characterization

The PEC electrode is characterized using X-ray photoelectron spectroscopy (XPS), X-ray diffraction (XRD) and Scanning electron microscopy (SEM). For XPS measurements a Quantera SXM (scanning XPS microprobe) from Physical Electronics is used with monochromatic Al Kα excitation. For XRD analysis the X'Pert Powder Pro from PANalytical is used with Cu Kα irradiation (λ = 0.15 nm). Diffraction patterns are recorded between $5 \leq 2\theta \leq 80$. SEM images are obtained with a Jeol JSM7610 FEG SEM.

2.3. Electrochemical and photo-electrochemical characterization of hematite and NiOOH/hematite

Initial tests are performed in a simple beaker glass using the NiOOH/hematite electrode as working electrode, a Pt counter electrode and a Hg/HgO (1 M NaOH) liquid junction reference electrode (EF1369, BASi Research Products). Cyclic voltammetry, at a scan speed of 50 mV/s is performed using a Bio-logic potentiostat (Bio-logic SP300) in the potential range from − 0.5–0.8 V vs. Hg/HgO reference electrode. LEDs (460 nm, buyledstrips.nl) are wrapped around the beaker for illumination of the sample. The optical power density inside the beaker is measured using a silicon photodiode (S121C, Thorlabs) connected to an optical power measurement module (PM100USB, Thorlabs). Different driving voltages (18–24 V) are used for the LEDs and the corresponding power density is measured in the center of the beaker with a maximum of 15.0 mW/cm^2. Urea (U5128 99.0 – 100.5%, Sigma Aldrich) concentrations of 0, 25, 100, and 250 mM are measured in dark and illuminated conditions with background electrolytes of 100 mM NaCl (S5886, ≥99%, Sigma Aldrich) and 1 M NaOH (S8045 ≥98%, Sigma Aldrich). Furthermore, the performance of a bare hematite substrate is compared to a NiOOH coated hematite substrate, using cyclic voltammetry in various solutions containing 1 M NaOH, 1 M NaOH + 100 mM NaCl, and 1 M NaOH + 100 mM NaCl + 50 mM urea. The influence of the pH on PEC urea oxidation is investigated by performing PEC urea oxidation in a narrow pH range (11−14) using electrolyte solutions containing 25 mM urea and 100 mM NaCl. Finally, PEC urea oxidation experiments are performed under various illumination intensities in a solution containing 1 M NaOH, 100 mM NaCl and 50 mM urea.

2.4. Static PEC urea oxidation measurements

The PEC device for the static urea removal tests, as shown in Fig. 2 is made out of a polydimethylsiloxane (PDMS) spacer that is fixed on top of

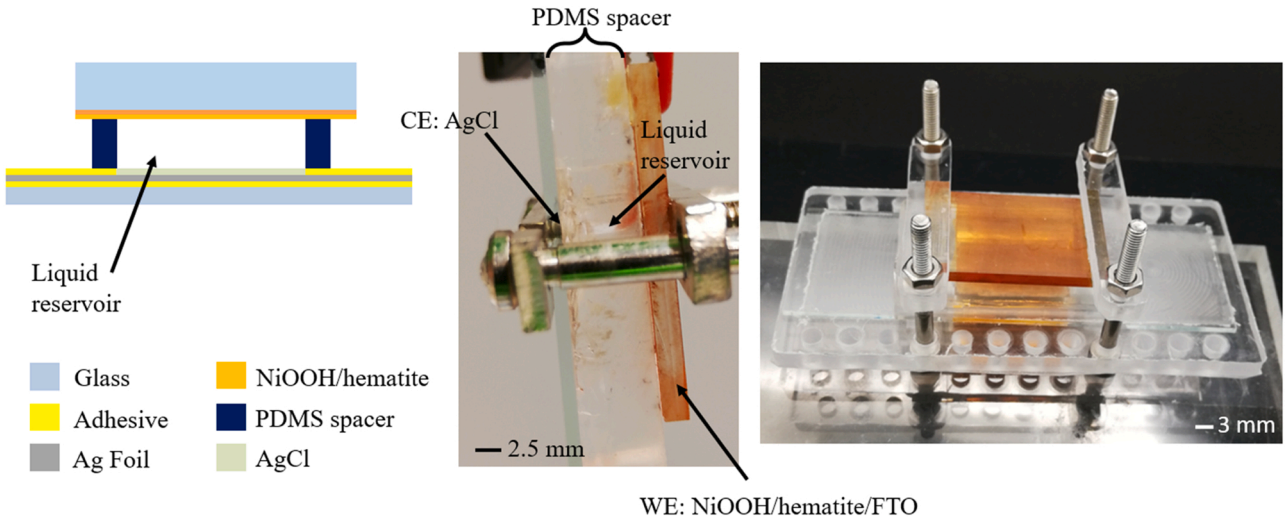

Fig. 2. On the left a schematic overview of the static PEC oxidation urea cell. The PEC electrode with the photosensitive hematite layer and the NiOOH catalyst are shown. The counter electrode consists of a chlorinated piece of silver foil attached to a glass slide using pressure sensitive, double-sided, adhesive tape. In between is a PDMS spacer that is attached to the silver foil using the same adhesive tape. On the right the micromilled clamp is shown that allows illumination of the PEC electrode through the FTO/glass side.

a microscopy slide containing chlorinated silver foil (AgCl) using pressure sensitive tape (ARSeal 90880, Adhesives Research Inc.). The PEC working electrode is clamped on top of the PDMS. The reaction chamber in the PDMS cell is 20 × 10×6 mm. The total volume inside this reaction chamber is 1.2 mL Blue LEDs are used to illuminate the NiOOH/hematite/FTO electrode from the FTO/glass side. The LEDs are arranged on an aluminum square. The optical power output is measured as a function of distance and fixed at an optical power of 18.2 mW/cm^2 for all experiments. The current is measured using a potentiostat (EM Stat, Palm Instruments BV, and PSTrace 4.8 software) during 4 separate runs of urea oxidation ranging from 2 to 4 h. A solution containing 50 mM urea, 100 mM NaCl and 1 M NaOH is used for these experiments. The analysis of urea conversion has been performed after individual experiments. The remaining solution is collected and titrated back to pH 7 using a Mettler Toledo Sevenmulti pH meter and 1 M HCl (258148 37%, Sigma Aldrich) solution. It is noted that less HCl needs to be added to the treated samples when compared to the untreated sample, as the OH^- ions have been used in the reactivation of the catalyst. Furthermore, the generated CO_2 forms bicarbonate ions in this alkaline environment, which also decreases the pH. On average the treated samples need 0.94 mL/mL of HCl versus 0.98 mL/mL for the stock solution. For a theoretical calculation on the removed urea the Faradaic current can be converted into the removed moles of urea by using the fact that 6 electrons are used in converting a single urea molecule. The Faraday constant (96485 C/mol) is used to correlate the current passed through the system to the removed amount of urea. The urea concentration is measured in the clinical laboratory of the hospital.

The PDMS spacer is made using a PMMA mold. For the PDMS a weight ratio of 10:1 of liquid pre-polymer vs curing agent is used (Sylgard 184, Dow Corning). The solution is degassed for 30 min in a desiccator at 200 mbar and poured on top of the PMMA mold. The PDMS is thermally cured for 4 h at 60 °C and removed from the mold. The PMMA clamp and mold are made with a Datron neo next milling machine.

2.5. Gas product detection using mass-spectrometry during PEC urea oxidation

To detect the formation of N_2 gas during the selective PEC oxidation of urea, mass spectrometry experiments are performed. For these experiments an adapted version of the static cell shown in Fig. 2 is fabricated that does allow flow (for further details see SI.B). A solution of 50 mM urea, 100 mM NaCl and 1 M NaOH is circulated at a flow rate of 3.3 mL/min using a peristaltic pump (Ismatec). The substrate is illuminated through the FTO/glass side at 22.5 mW/cm^2. The gasses leaving the reactor and entering the sample vial are analyzed by mass spectrometry (SpectroInlets).[29–32] The products of interest (N_2, O_2, CO_2, Cl_2, NH_3) were detected according to their mass-to-charge ratio (m/z). Signals were recorded over time.

2.6. Liquid phase analysis

To detect the formation of nitrite and nitrate ion chromatography is performed on a treated sample. In a typical experiment 1.3 mL of a 50 mM urea and 1 M NaOH is used treated in the static flow cell. The PEC urea oxidation, without external bias is performed for 2 h. The sample is illuminated through the FTO/glass side at 18.2 mW/cm^2. The collected sample is analyzed by a Methrom ion chromatograph with a Metrosep A Supp 16 – 150/4 column. Calibration curves for nitrite and nitrate are obtained using standard solutions in the concentration range 0.5–5 mM for nitrite and 0.5–4 mM for nitrate.

3. Results and discussion

3.1. Characterization of the hematite and NiOOH/Ni(OH)$_2$ catalyst

SEM, XRD and XPS characterization of the substrate confirm the successful growth of hematite nanorods and the deposition of the NiOOH/Ni(OH)$_2$ on its surface. SEM images of a substrate containing the hydrothermally grown hematite nanorods are depicted in Fig. 3a, where Fig. 3b shows the sample after electrodeposition of NiOOH//Ni(OH)$_2$ (at −0.65 V vs Ag/AgCl (sat'd KCl) for 120 s). Only a partial co-catalysts coverage has been achieved, where literature shows a more uniform co-catalyst deposition for a fixed current deposition technique [14]. For the used fixed potential deposition, larger nickel domains seem to have formed. This does not seem to effect the catalytic activity. Fig. 3c shows the XRD spectra for two substrates. The observed diffraction lines are indicative of α-hematite (labeled with a +), [14] the FTO layer and the underlying glass substrate, respectively. Similar to Xu et al. [14] the NiOOH is not detected in the XRD spectrum, likely due to the low crystallinity and thickness of electrodeposited NiOOH [14] Finally the XPS spectra shows Fe2p$_{3/2}$ peaks around 710.35 eV that are

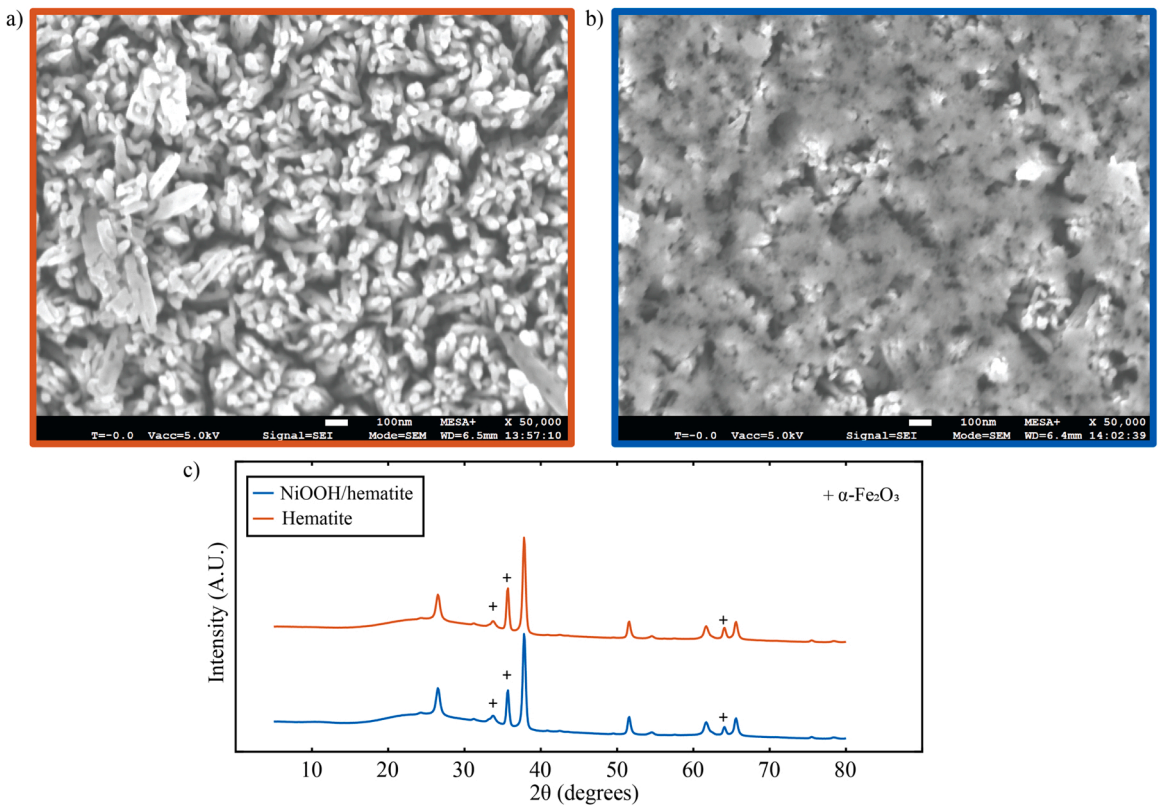

Fig. 3. SEM images of a) hydrothermally grown hematite nanorods and b) the electrodeposited NiOOH catalyst (−0.65 V vs Ag/AgCl (sat'd KCl) for 120 s) on top of the hematite nanorods. XRD pattern, c), showing the analysis for a substrate containing only hydrothermally deposited hematite (red line) and the electrodeposited catalyst (−0.65 V vs Ag/AgCl (sat'd KCl) for 120 s) on top of the hematite. The lines indicative for α-hematite are indicated with a + . The other peaks are contributed to the FTO electrode and the elevated baseline between $15 \leq 2\theta \leq 35$ is most likely due to the glass substrate.

characteristic for hematite [33]. The spectra for $Ni2p_{1/2}$ and $Ni2p_{3/2}$ are indicative of $Ni(OH)_2$. An additional scan of the Ni3d and O2s region further confirmed the presence of β-$Ni(OH)_2$. The survey spectra and more details about the Fe2p, Ni2p, Ni3d and O2s regions are summarized in figure C.1 [34].

3.2. *Electrochemical and photo-electrochemical properties of NiOOH/Hematite and Hematite*

Initial photo-electrochemical tests are conducted to determine the influence of the NiOOH catalyst on the (photo)electrochemical properties of hematite photo-electrodes. Fig. 4 shows cyclic voltammetry scans where it is shown that in Fig. 4a-b the presence of NaCl causes no increased oxidation current when compared to the scan without the presence of NaCl for both dark and illuminated conditions. This suggests that there is no significant influence or competition of chloride oxidation, especially when compared to the influence of adding urea in Fig. 4c. However, there is a small shift in the reduction potential visible in Fig. 5b when compared to Fig. 4a. In both cases the addition of the NiOOH catalyst causes the onset potential for the oxidation peak to shift to ~0.45 V, as shown in Fig. 4a-b, which is contributed to water splitting on the catalyst. On the backwards scan, a reduction peak is observed around ~0.2 V indicating deactivation of the catalyst to $Ni(OH)_2$. When both NaCl and urea are present, Fig. 5c, it is observed that under illumination conditions, the oxidation onset potential shifts towards ~− 0.4 V. Due to the absence of this shift in illuminated conditions without urea, it is shown that the combination of the hematite with the NiOOH catalyst favors urea oxidation in the potential window from − 0.4–0.5 V. From 0.5 V onwards the added energy from the potentiostat in addition to the photo-induced voltage causes the current to increase further. Current densities are lower than reported in literature. However, illumination intensities of 100 mW/cm^2 are used in that case [15]. Fig. 5a shows cyclic voltammograms of PEC urea oxidation on a NiOOH/hematite substrate for different illumination conditions. When looking at the current density at 0.2 V for each illumination intensity in Fig. 5b, it can be seen that with a higher illumination intensity the current density increases, as more electron-pairs are generated. Based on the obtained data, the current density appears to reach a plateau for much higher illumination intensities. However, in literature other photo-sensitive materials are reported to have a linear characteristic with the illumination intensity for a much larger intensity range [35]. It is expected that the hematite will behave the same, however that is limited by the relatively low intensities used in this graph.

Using dark conditions (figure D.1) and constant illumination, Fig. 6a) and b), the influence of urea concentrations and pH on the current-potential profile has been evaluated. The effect of urea concentration, Fig. 6a) is primarily shown by a small increase in photocurrent as observed in the potential region from 0 V to 0.4 V. The observed current difference in forward and backward scan indicates that with increasing urea concentration transport limitations are mitigated. Nevertheless, the data clearly reveal that even small amounts of urea are oxidized in the presence of the NiOOH/hematite photo-electrode. Contrasting the observed minor impact of urea concentration the changes in the electrolyte pH has a significant impact on the current-potential response of the system. As shown in Fig. 6b) with decreasing pH, the measured photocurrent drops. Likely, catalyst reactivation is insufficient for solutions with a pH < 12. Similarly, in the dark for electrolyte solutions with a pH < 12, there is no noteworthy current related to urea oxidation observed (figure D.1), further emphasizing that strongly alkaline conditions are required for reactivation of the nickel catalyst.

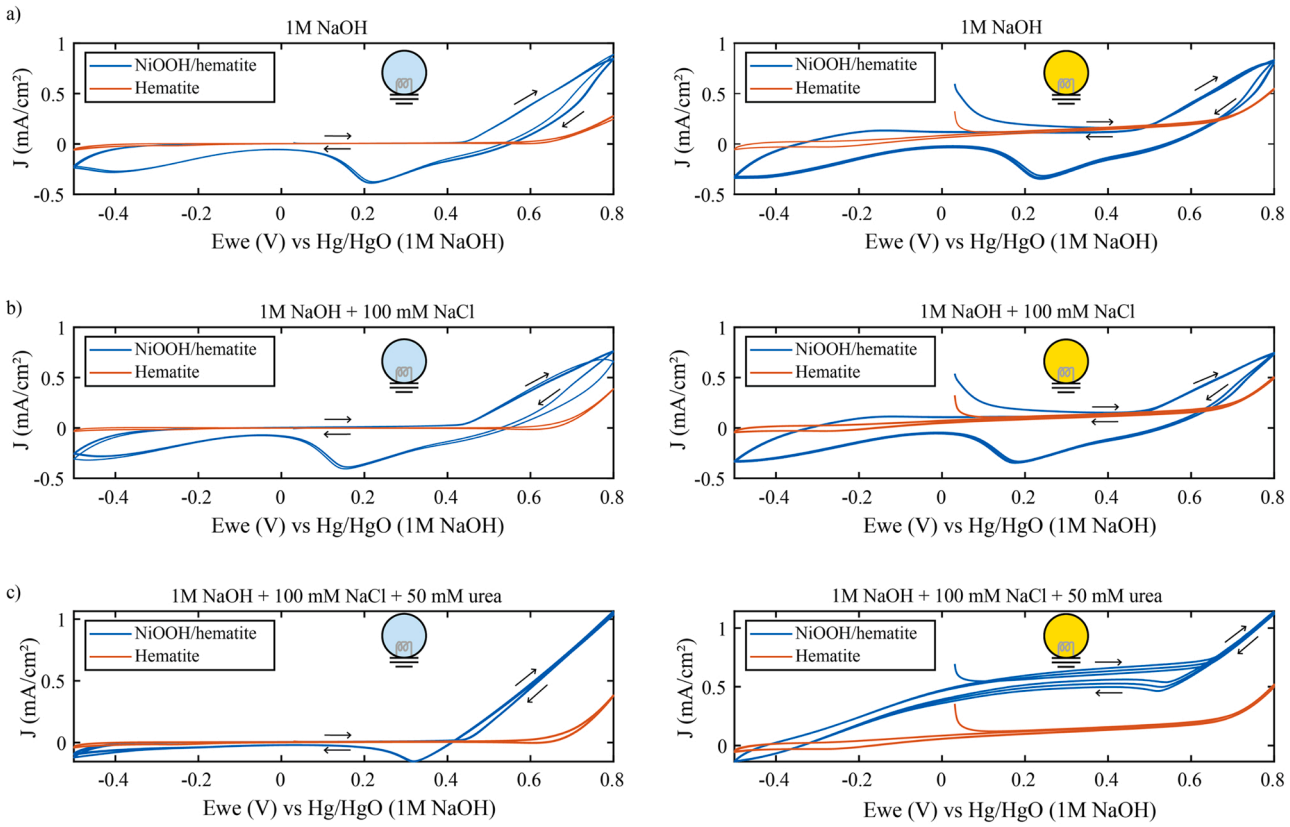

Fig. 4. Cyclic voltammograms under dark and illuminated (460 nm at 15.0 mW/cm^2) conditions of a bare hematite and NiOOH/substrate vs a Hg/HgO (1 M NaOH) reference electrode and a Pt counter electrode. Scans a performed at a rate of 50 mV/s. The solutions contain a) 1 M NaOH, b) 1 M NaOH and NaCl, and c) 1 M NaOH, 100 mM NaCl and 50 mM urea. Arrows indicate the scan direction.

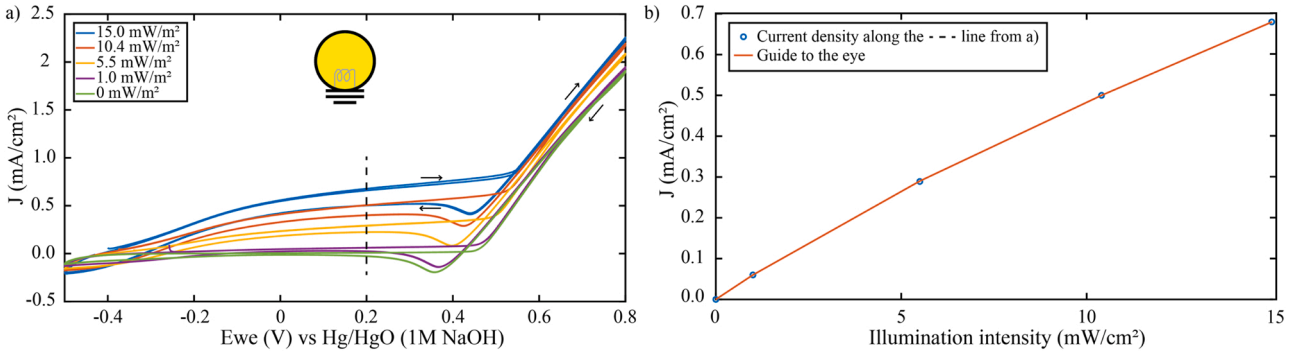

Fig. 5. Cyclic voltammograms under different illumination intensities a) (460 nm at 0, 1, 5.5, 10.4, and 15.0 mW/cm^2) of a NiOOH/hematite substrate vs a Hg/HgO (1 M NaOH) reference electrode and a Pt counter electrode. Scans are performed at 50 mV/s. The used solution contains 1 M NaOH, 100 mM NaCl and 50 mM urea. Arrows indicate the scan direction. The current densities at 0.2 V from a) are plotted versus the illumination intensity b). The blue dots show the individual data points and the red line a guide for the eye to visualize the trend.

3.3. PEC urea oxidation in a static cell using AgCl counter electrodes

PEC urea oxidation using the NiOOH/hematite substrates were shown to enable light driven urea oxidation. Yet, using Pt counter electrodes the application of an additional bias was mandatory. Replacing Pt counter electrodes with a AgCl counter electrode resulted in solely light-driven urea oxidation. As shown in Fig. 7, in the presence of Pt counter electrodes the photo-induced voltage is not high enough for the reaction to occur as evidenced by the absence of any significant current when the LEDs are switch on. Using a AgCl counter electrode instead, an immediate response to LED illumination is observed even in the absence of an external applied bias. Thus using silver-chloride reduction (equation Eq.3) as counter reaction is essential for the development of a self-powered device.

The selectivity for light-driven urea removal was tested by performing multiple removal runs in a static cell equipped with the NiOOH/hematite photo-electrode and a AgCl counter electrode. Fig. 7b) shows a 4 h run revealing the stability of the photo-electrode (see figure E.1 for other runs) and highlighting again that solely LED illumination is used to drive the oxidation reaction as in the absence of light the measured current drops to 0 mA. For the first two runs the AgCl reduction was run till the layer was depleted and the current drops in those cases as well, demonstrating no other reaction with the silver substrate is occurring. These runs are shown in figure E.1. All runs are performed with the same

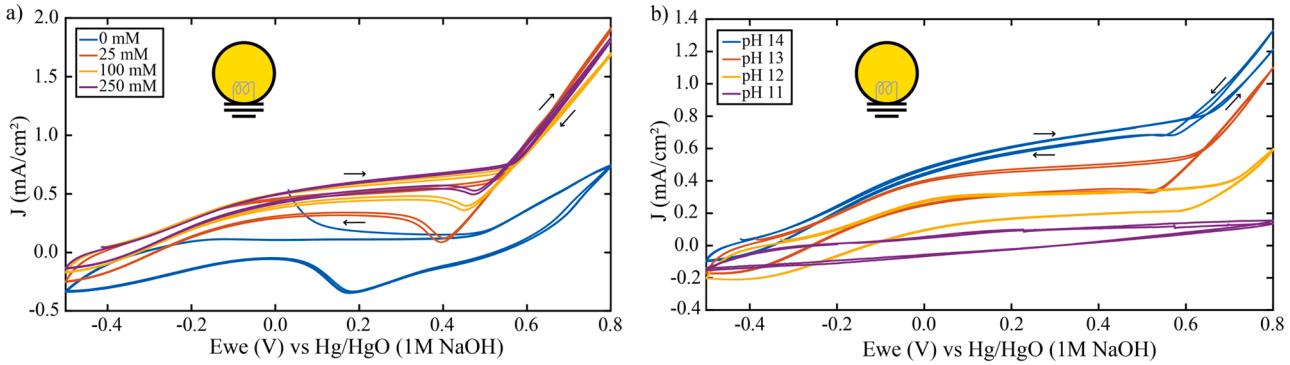

Fig. 6. Cyclic voltammograms showing two scans of PEC urea oxidation on a NiOOH/hematite substrate vs a Hg/HgO (1 M NaOH) reference electrode and a Pt counter electrode. Different urea concentrations a) (0, 25, 100, and 250 mM) are used at pH 14 containing 100 mM NaCl illuminated conditions (460 nm at 15 mW/cm^2). Furthermore, different pH conditions b) (pH 11–14) with 100 mM NaCl and 50 mM urea under illuminated conditions (460 nm at 15.0 mW/cm^2) are tested. Arrows indicate the forward and reverse scan direction.

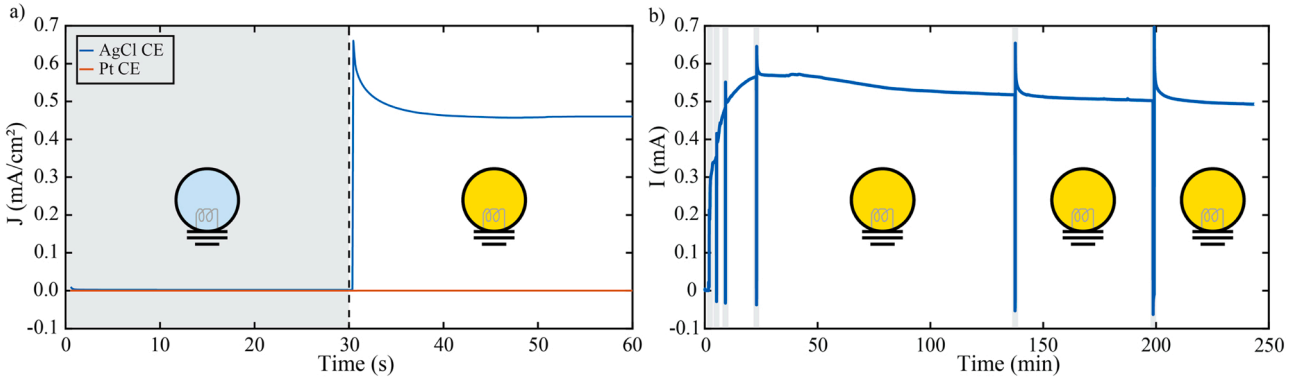

Fig. 7. In a) a comparison of PEC urea oxidation on a NiOOH/hematite substrate using a Pt counter electrode (red line) and a AgCl counter electrode (blue line). A solution containing 1 M NaOH, 100 mM NaCl and 50 mM urea is used in both cases. LEDs (460 nm at 15.0 mW/cm^2) are switched on after 30 s. No external bias voltage is applied. In b) light-driven urea oxidation runs show the current over 4 h. The spikes indicate the on/off switching of the LEDs (460 nm at 18.5 mW/cm^2) showing that the current goes down to 0 mA when the light is off. No external bias voltage is applied. A solution (1.2 mL) containing 50 mM or urea, 100 mM NaCl and 1 M of NaOH is used.

PEC electrode, demonstrating the reusability of the electrode. From literature it is known that electrochemically grown and low crystalline (or amorphous) $Ni(OH)_2$ is a mechanical and electrochemical stable material [36–38]. A comparison of the theoretical urea removal estimated by charge passed through the system and the actual urea removal determined by back-titration is summarized in Table 1. The good agreement confirms the selectivity of urea removal obtained by the photo-electrochemical approach. The average removal rate for all the runs is 2.5 μmol/cm^{2}h (or 0.15 mg/cm^{2}h). For removing the daily produced amount of ~300 mmol of urea, this would extrapolate to a total surface area of 0.5 m^2 when operated for 24 h. This footprint can be reduced by improving the topological surface structure, creating more available surface per cm^2 and/or by optimizing the surface to volume ratio of the flow cell by closer spacing of the electrodes.

Table 1
Urea concentrations for the different PEC urea oxidation runs and the stock solutions. The prepared urea concentration at the start of each run is shown as well as the theoretical concentrations after the PEC runs and after subsequent back-titration using 1 M HCl. Finally, the measured urea concentrations are shown in the last row (n = 2).

	Run 1	Run 2	Run 3	Run 4	Stock
Prepared [urea] before PEC oxidation (mM)	50	50	50	50	50
Theoretical [urea] after PEC oxidation (mM)	44.1	43.8	43.4	40	50
Theoretical [urea] after back-titration using 1 M HCl (mM)	22.8	22.1	22.3	20.8	25.1
Measured average [urea] (mM) n = 2	22.6	22.3	22.4	20.9	25

To finally also validate the selectivity towards non-toxic products, i.e. N_2 and CO_2, head space analysis of the collected gasses collected using mass-spectrometry and ion chromatography to detect NO_2^- and NO_3^- have been performed (see SI.F for details of used system). Under illumination of the PEC electrode during the mass-spectrometry experiments, bubble formation at the surface of the working electrode was observed. Fig. 8 shows the response of the individual mass-to-charge signals after injection. Specifically, NH_3, N_2, O_2, Cl_2, and CO_2 were recorded over the duration of the measurement. Switching the LEDs on and off did not result in a directly measurable signal because of trapping of gas bubbles at the surface of the electrode, as illustrated in figure B.1. Still, bubble detachment resulted in the measurement of a transient signal, of both nitrogen and oxygen. While the oxygen signal was mainly caused by residual atmospheric air bubbles that were still stuck in the chip as well as some residual degassing of the liquid due to the increased temperature caused be the LEDs, the disproportional increase of the nitrogen signal indicated the formation of N_2 at the PEC surface. The absence of measurable amounts of CO_2 can be rationalized by the favorable formation of bicarbonate in the alkaline environment that is used. Importantly, there is no increase in NH_3 or Cl_2 signals, which further supports the selectivity of the PEC urea oxidation method over chloride oxidation.

The ion chromatography experiments show a nitrite concentration of

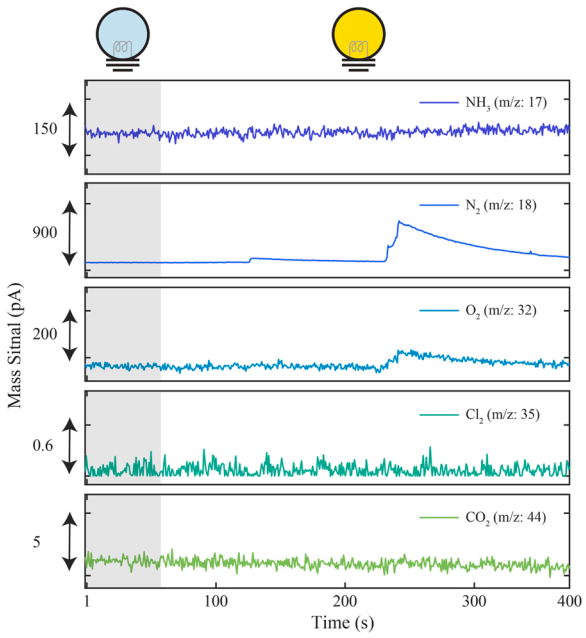

Fig. 8. Mass-spectrum signals of the products of interest of the headspace analysis during PEC urea oxidation on a NiOOH/hematite substrate using a AgCl counter electrode. No external bias voltage is applied. A solution containing 50 mM urea, 100 mM NaCl and 1 M NaOH is used. The LEDs (460 nm at 22.5 mW/cm^2) are switched on after 60 s. An increase in N_2 and O_2 is observed when a PEC generated bubble enters the sample vial and is analyzed. There is no signal detected for NH_3, Cl_2 or CO_2.

0.42 mM, which corresponds to a Faradaic efficiency of 39%. No significant amount of nitrate or other anions where detected besides chloride, which was formed at the counter electrode. Overall the results obtained demonstrate the selectivity of the NiOOH/hematite PEC urea oxidation over chloride oxidation in an alkaline environment and reveal the potential of the process to convert urea. "However, recent publications reveal that both nitrites and nitrates, as well as cyanate are formed in measurable quantities, [39–41] limiting urea conversion to N_2 to Faradaic efficiencies of 10–18% in the worst case [39,41] .Further research has to focus on the improvement of the selectivity of urea oxidation for N_2 generation over nitrite (no nitrate is detected in our study) or a strategy to efficiently remove generated nitrite. In fact, finding more efficient urea oxidation catalysts for increased current density and efficiency for waste water treatment and hydrogen formation is a developing research field with improvements made on a regular basis [42–46]. Recently, Cu has been shown to increase the formation of N_2 over NO_2^- [39,40]. Similarly, addition of polymers was shown to be beneficial for N_2 formation [39]. As mentioned by Rebiai et al., 2023, [41] optimization of electrochemical conditions regarding the applied potential or the overall process operation (e.g. pulsed potential or chopped light illumination) may improve selectivity for N_2 over nitrite generation. Nitrite accumulation can also be prevented by effective removal of produced nitrite using either sorbents (e.g. hydrotalcite based sorbents [47]) or post-treatment conversion (oxidation) of nitrite into nitrate [48,49], which is less toxic and can in its turn be efficiently removed with sorbents (e.g. hydrotalcite(-like) [47,50] or biomass derived sorbents [51]).

Furthermore, a focus on the selectivity of urea oxidation over other molecules present in the spent dialysate, such as glucose and small plasma proteins, has to be researched. Glucose oxidation products, for example, caused bio-compatibility issues in the past [8]. NiOOH catalysts show affinity for nitrogen containing compounds, however, they can still oxidize glucose. Aquaporin based membranes have been shown to be able to separate urea from glucose in a forward osmosis setup [52]. The light-driven reaction gives perspective of making a compact continuous flow micro-photo reactor as earlier proposed by Noel, 2017 [53]. To enable long-lasting of a WAK device, further improvements are still required. Especially, the capacity of the used AgCl electrode is limited and recharging is required. This can, for example, be done by developing an exchangeable counter electrode cartridge that can be disconnected from the WAK and replaced with a new counter electrode. The spent counter electrode can be regenerated externally. Alternatively, a platinum electrode could be integrated in the WAK as a third electrode which can be used to recharge the AgCl electrode while still integrated in the WAK and when it is not in use for dialysis. Although it was shown that the reaction did not continue when the AgCl was depleted, it has to be investigated whether silver ions leach into the solution which may cause further bio-compatibility issues. The pH of the regeneration fluid can be kept above pH 12 by adding NaOH pellets or replacing the entire volume when the pH becomes too low. Another issue is the highly alkaline environment that is not (bio)compatible with an artificial kidney system at the moment. One possible solution to solve this is to introduce an extra loop to the WAK system that can isolate the high pH side from the patient side and at the same time allow urea to reach this loop, using for example cation exchange/anion rejection membranes. These membranes, that are used commonly in e.g. electrochemical fuel cells, have negatively charged surface groups that prevent anions to diffuse through, but allows transport of neutral substances (such as urea) and positively charged species [54,55]. Finally, the release of chloride ions is problematic for a WAK as it may cause hyperchloremic acidosis in the patient. The aforementioned ion rejection membranes can block the chloride ions that are released at the counter electrode as well.

4. Conclusion

A light-driven photo-electrocatalytic method for selective and direct urea oxidation with the intended use in a wearable artificial kidney has been presented. By using a AgCl counter electrode the photo-induced voltage suffices to drive the reaction and no external bias is required. Selectivity over chloride oxidation and water splitting is shown by characterization of the NiOOH/hematite PEC electrode in alkaline solution (pH 14) both with and without urea and NaCl in dark and illuminated conditions. Selectivity of the process over chloride oxidation is confirmed for extended duration by measuring the removed amount of urea and by detection of N_2 formation. No unwanted side-products such as ammonia, nitrate or chlorine were detected. An average removal rate of 2.5 μmol/cm^{2}h (or 0.15 mg/cm^{2}h) is obtained, meaning that a surface area of 0.5 m^2 would be sufficient to remove the daily amount of ~300 mmol of urea. However, nitrite formation was observed, and further work should thus focus on enhancing N_2 over NO_2^- selectivity.

CRediT authorship contribution statement

J.C.V. designed and fabricated the PEC substrates and the flows cells, and performed and designed the initial urea removal experiments. Data processing for these experiments is performed by J.C.V., with reviewing of K.G.F.G. and M.O. A.P.R. and J.C.V. performed and designed the mass-spec experiments, where A.P.R. did the data processing. A first version of the manuscript was written by J.C.V. and A.P.R. with extensive reviewing and editing by B.M. B.M., M.O., K.G.F.G, M.C.V, and G.M. performed further editing and review of the manuscript including revisions. K.Z. and J.C.V. performed the ion chromatography experiments. The idea for novel technologies and dialysate regeneration by means of EO for a WAK is conceptualized by K.G.F.G., where the use of (photo)-electrocatalysts in this context is conceptualized by J.C.V. and M.O.

Declaration of Competing Interest

The authors declare that they have no known competing financial interests or personal relationships that could have appeared to influence

the work reported in this paper.

Data Availability

Data will be made available on request.

Acknowledgements

All authors acknowledge the financial support of the strategic alliance of the University of Twente, University Medical Center Utrecht and Utrecht University. The authors would like to thank and acknowledge Gerard Kip for his help in performing the XPS experiments and data processing, Harry Bakker and Karin van Nieuwenhuijzen for their help in performing XRD experiments and data processing, and Johan Bomer for his help in taking SEM images. Erna Fränzel-Luiten and Kim Zijderveld are acknowledged for their support with the ion chromatography experiments.

Appendix A. Supporting information

Supplementary data associated with this article can be found in the online version at doi:10.1016/j.cattod.2023.114163.

References

[1] M.K. van Gelder, et al., Urea removal strategies for dialysate regeneration in a wearable artificial kidney, Biomaterials 234 (2020), 119735.
[2] G. Shao, J. Himmelfarb, B.J. Hinds, Strategies for optimizing urea removal to enable portable kidney dialysis: a reappraisal, Artif. Organs 46 (2022) 997–1011.
[3] M.J. Blumenkrantz, et al., Applications of the Redy® sorbent system to hemodialysis and peritoneal dialysis, Artif. Organs 3 (1979) 230–236.
[4] J.A.W. Jong, et al., A ninhydrin-type urea sorbent for the development of a wearable artificial kidney, Macromol. Biosci. 20 (2020).
[5] J.A.W. Jong, et al., Phenylglyoxaldehyde-functionalized polymeric sorbents for urea removal from aqueous solutions, ACS Appl. Polym. Mater. 2 (2020) 515–527.
[6] M. Wester, et al., Removal of urea by electro-oxidation in a miniature dialysis device: a study in awake goats, Am. J. Physiol. - Ren. Physiol. 315 (2018) F1385–F1397.
[7] M. Wester, et al., Removal of urea in a wearable dialysis device: a reappraisal of electro-oxidation, Artif. Organs 38 (2014) 998–1006.
[8] M.K. van Gelder, et al., Safety of electrooxidation for urea removal in a wearable artificial kidney is compromised by formation of glucose degradation products, Artif. Organs 45 (2021) 1422–1428.
[9] R. Brüninghoff, et al., Comparative analysis of photocatalytic and electrochemical degradation of 4-ethylphenol in saline conditions, Environ. Sci. Technol. 53 (2019) 8725–8735.
[10] G. Shao, Y. Zang, B.J. Hinds, TiO2 nanowires based system for urea photodecomposition and dialysate regeneration, ACS Appl. Nano Mater. 2 (2019) 6116–6123.
[11] D. Dector, et al., Harvesting energy from real human urine in a photo-microfluidic fuel cell using TiO2–Ni anode electrode, Int. J. Hydrog. Energy 46 (2021) 26163–26173.
[12] S. Park, J.T. Lee, J. Kim, Photocatalytic oxidation of urea on TiO 2 in water and urine: mechanism, product distribution, and effect of surface platinization, Environ. Sci. Pollut. Res. 26 (2019) 1044–1053.
[13] B. Zhu, Z. Liang, R. Zou, Designing advanced catalysts for energy conversion based on urea oxidation reaction, Small 1906133 (2020) 1–19.
[14] D. Xu, et al., A Ni(OH)2-modified Ti-doped α-Fe2O3 photoanode for improved photoelectrochemical oxidation of urea: the role of Ni(OH)2 as a cocatalyst, Phys. Chem. Chem. Phys. 17 (2015) 23924–23930.
[15] G. Wang, et al., Solar driven hydrogen releasing from urea and human urine, Energy Environ. Sci. 5 (2012) 8215–8219.
[16] R.K. Singh, K. Rajavelu, M. Montag, A. Schechter, Advances in catalytic electrooxidation of urea: a review, Energy Technol. 9 (2021) 1–28.
[17] D. Liu, et al., High-performance urea electrolysis towards less energy-intensive electrochemical hydrogen production using a bifunctional catalyst electrode, J. Mater. Chem. A 5 (2017) 3208–3213.
[18] K. Ye, G. Wang, D. Cao, G. Wang, Recent advances in the electro-oxidation of urea for direct urea fuel cell and urea electrolysis, Top. Curr. Chem. 376 (2018).
[19] T.W. Kim, K.S. Choi, Improving stability and photoelectrochemical performance of bivo4 photoanodes in basic media by adding a ZnFe2O4 layer, J. Phys. Chem. Lett. 7 (2016) 447–451.
[20] T. Saison, et al., New insights into BiVO4 properties as visible light photocatalyst, J. Phys. Chem. C. 119 (2015) 12967–12977.
[21] J. Juodkazytė, et al., Electrolytic splitting of saline water: durable nickel oxide anode for selective oxygen evolution, Int. J. Hydrog. Energy 44 (2019) 5929–5939.
[22] F. Dionigi, T. Reier, Z. Pawolek, M. Gliech, P. Strasser, Design criteria, operating conditions, and nickel-iron hydroxide catalyst materials for selective seawater electrolysis, ChemSusChem 9 (2016) 962–972.
[23] V. Vedharathinam, G.G. Botte, Direct evidence of the mechanism for the electro-oxidation of urea on Ni(OH)2 catalyst in alkaline medium, Electrochim. Acta 108 (2013) 660–665.
[24] V. Vedharathinam, G.G. Botte, Understanding the electro-catalytic oxidation mechanism of urea on nickel electrodes in alkaline medium, Electrochim. Acta 81 (2012) 292–300.
[25] B. Zhu, Z. Liang, R. Zou, Designing advanced catalysts for energy conversion based on urea oxidation reaction, Small 1906133 (2020) 1–19.
[26] B. Ash, V.S. Nalajala, A.K. Popuri, T. Subbaiah, M. Minakshi, Perspectives on nickel hydroxide electrodes suitable for rechargeable batteries: Electrolytic vs. chemical synthesis routes, Nanomaterials 10 (2020) 1–22.
[27] P. Wang, et al., Efficient hydrogen generation and total nitrogen removal for urine treatment in a neutral solution based on a self-driving nano photoelectrocatalytic system, Nanomaterials 11 (2021).
[28] Bard, A.J. Standard Potentials in Aqueous Solution. (1985). doi:doi/10.1201/9780203738764.
[29] D.B. Trimarco, et al., Enabling real-time detection of electrochemical desorption phenomena with sub-monolayer sensitivity, Electrochim. Acta 268 (2018) 520–530.
[30] D.B. Trimarco, T. Pedersen, O. Hansen, I. Chorkendorff, P.C.K. Vesborg, Fast and sensitive method for detecting volatile species in liquids, Rev. Sci. Instrum. 86 (2015), 075006.
[31] P.M. Krzywda, et al., Electroreduction of NO3− on tubular porous Ti electrodes, Catal. Sci. Technol. (2022) 3281–3288, https://doi.org/10.1039/d2cy00289b.
[32] P.M. Krzywda, A. Paradelo Rodríguez, N.E. Benes, B.T. Mei, G. Mul, Effect of electrolyte and electrode configuration on Cu-catalyzed nitric oxide reduction to ammonia, ChemElectroChem 9 (2022) 1–7.
[33] (NIST), National Institute of Standards and Technology. Available at: https://srdata.nist.gov/xps/XPSDetailPage.aspx?AllDataNo=26539. (Accessed: 31st October 2022).
[34] A.N. Mansour, Characterization of β-Ni(OH)2 by XPS. in, Surf. Sci. Spectra 3 (1994).
[35] W. Niu, et al., Extended light harvesting with dual Cu2O-based photocathodes for high efficiency water splitting, Adv. Energy Mater. 8 (2018).
[36] S.L. Medway, C.A. Lucas, situ Stud. Oxid. Nickel Electrodes Alkaline Solut. 587 (2006) 172–181.
[37] Y. Su, K. Xiao, N. Li, Z. Liu, S. Qiao, pseudocapacitors asymmetric supercapacitors (2014) 13845–13853, https://doi.org/10.1039/c4ta02486a.
[38] S. Trafela, J. Zavasnik, S. Sturm, K.Z. Rozman, Formation of a Ni (OH) 2 / NiOOH active redox couple on nickel nanowires for formaldehyde detection in alkaline media, Electrochim. Acta 309 (2019) 346–353.
[39] J. Li, et al., Deciphering and suppressing over-oxidized nitrogen in nickel-catalyzed urea electrolysis, in: Chemie- Int (Ed.), Angew, 60, 2021, pp. 26656–26662.
[40] S.W. Tatarchuk, J.J. Medvedev, F. Li, Y. Tobolovskaya, A. Klinkova, Nickel-catalyzed urea electrolysis: from nitrite and cyanate as major products to nitrogen, Evol. Angew. Chem. Int. Ed. 61 (2022).
[41] L. Rebiai, et al., Photoelectrocatalytic conversion of urea under solar illumination using Ni decorated Ti-Fe2O3 electrodes, Electrochim. Acta 438 (2023), 141516.
[42] J. Dabboussi, et al., Solar-assisted urea oxidation at silicon photoanodes promoted by an amorphous and optically adaptive Ni-Mo-O catalytic layer, J. Mater. Chem. A 10 (2022) 19769–19776.
[43] T. Yu, et al., Boosting urea-assisted water splitting by constructing sphere-flower-like NiSe2-NiMoO4 heterostructure, Chem. Eng. J. 449 (2022), 137791.
[44] X. Zhuo, et al., Ni3S2/Ni heterostructure nanobelt arrays as bifunctional catalysts for urea-rich wastewater degradation, ACS Appl. Mater. Interfaces 13 (2021) 35709–35718.
[45] X. Zhuo, et al., Crystalline-amorphous Ni3S2-NiMoO4Heterostructure for durable urea electrolysis-assisted hydrogen production at high current density, ACS Appl. Mater. Interfaces 14 (2022) 46481–46490.
[46] J. Li, et al., A review of hetero-structured Ni-based active catalysts for urea electrolysis, J. Mater. Chem. A 10 (2022) 9308–9326.
[47] J. Chen, et al., Adsorption of nitrate and nitrite from aqueous solution by magnetic Mg/Fe hydrotalcite, Water Supply 21 (2021) 4287–4300.
[48] D. Chen, J. Jiang, X. Du, Electrocatalytic oxidation of nitrite using metal-free nitrogen-doped reduced graphene oxide nanosheets for sensitive detection, Talanta 155 (2016) 329–335.

[49] F. Armijo, et al., Electrocatalytic oxidation of nitrite to nitrate mediated by Fe(III) poly-3-aminophenyl porphyrin grown on five different electrode surfaces, J. Mol. Catal. A Chem. 268 (2007) 148–154.
[50] H. Zhou, Y. Tan, W. Gao, Y. Zhang, Y. Yang, Selective nitrate removal from aqueous solutions by a hydrotalcite-like absorbent FeMgMn-LDH, Sci. Rep. 10 (2020) 1–10.
[51] G.S. Nikolić, et al., Nitrate removal by sorbent derived from waste lignocellulosic biomass of lagenaria vulgaris: kinetics, equilibrium and thermodynamics, Int. J. Environ. Res. 15 (2021) 215–230.
[52] G. Shao, et al., Dialysate regeneration with urea selective membrane coupled to photoelectrochemical oxidation system, Adv. Mater. Interfaces 9 (2022) 1–8.
[53] T. Noël, A personal perspective on the future of flow photochemistry, J. Flow. Chem. 7 (2017) 87–93.
[54] R.S.L. Yee, R.A. Rozendal, K. Zhang, B.P. Ladewig, Cost effective cation exchange membranes: a review, Chem. Eng. Res. Des. 90 (2012) 950–959.
[55] S. Jiang, H. Sun, H. Wang, B.P. Ladewig, Z. Yao, A comprehensive review on the synthesis and applications of ion exchange membranes, Chemosphere 282 (2021), 130817.